Supporting Information for

Atomically Ordered Pt_3Mn Intermetallic Electrocatalysts for Oxygen Reduction Reaction in Fuel Cells

Jeonghoon Lim[1, †, ‡], Chanwon Jung[1, †, §], Doosun Hong[1], Junu Bak[1], Jaewook Shin[1], MinJoong Kim[1,2], DongHoon Song[1], Changsoo Lee[1,2], Jinkyu Lim[3], Hyunjoo Lee[3], Hyuck Mo Lee[1], and EunAe Cho[1,]*

[1]Department of Materials Science and Engineering, Korea Advanced Institute of Science and Technology (KAIST), 291 Daehak-ro, Yuseong-gu, Daejeon, 34141, Republic of Korea

[2]Hydrogen Research Department, Korea Institute of Energy Research (KIER), 152 Gajeong-ro, Yuseong-gu, Daejeon, 34129, Republic of Korea

[3]Department of Chemical and Biomolecular Engineering, Korea Advanced Institute of Science and Technology, Daejeon 34141, South Korea.

†J. Lim and C. Jung contributed equally to this work.

‡ *Current address: George W.Woodruff School of Mechanical Engineering, Georgia Institute of Technology, Atlanta, Georgia 30332, United States*

§ *Current address: Max-Planck-Institut für Eisenforschung GmbH, Düsseldorf 40237, Germany*

* Corresponding Author: eacho@kaist.ac.kr

Calculation of mass activity

The kinetic current (j_k) was calculated by using the Koutecky-Levich equation,[1] which is expressed by

$$j_k = \frac{j_d \times j}{|j_d - j|}, \frac{1}{j} = \frac{1}{j_k} + \frac{1}{j_d} = \frac{1}{j_k} + \frac{1}{0.62nF(D_{O_2})^{2/3}v^{-1/6}C_{O_2}\omega^{1/2}}$$

where j is the measured current density, j_d is the diffusion-limited current density, n is the number of electrons transferred, F is Faraday's constant (96,485 C mol^{-1}), D_{O2} is the diffusion coefficient of O_2 in 0.1 M $HClO_4$ solution (1.93×10^{-5} cm^2 s^{-1}), v is the kinematic viscosity of the electrolyte (1.01×10^{-2} cm^2 s^{-1}), C_{O2} is the concentration of oxygen in 0.1 M $HClO_4$ solution (1.26×10^{-6} mol cm^{-3}), and ω is the angular rate of the rotating disk electrode.

From calculated kinetic current, mass activity was calculated using below equation.

$$Mass\ activity = \frac{j_k}{m_{pt}}$$

where m_{Pt} is the total mass of Pt loaded on the electrode.

Calculation of electrochemically active surface area (ECSA)

ECSA was calculated by integration of the hydrogen adsorption region (Q_H) between 0.05 and 0.4 V_{RHE} using total mass of Pt loaded on the electrode (m_{Pt}) and 210 μC cm^{-2} of monolayer hydrogen adsorption charge on platinum (q_H) as follows.[2]

$$ECSA = \frac{Q_H}{m_{Pt} \times q_H}$$

Calculation of specific activity

$$Specific\ activity = \frac{Mass\ activity}{ECSA}$$

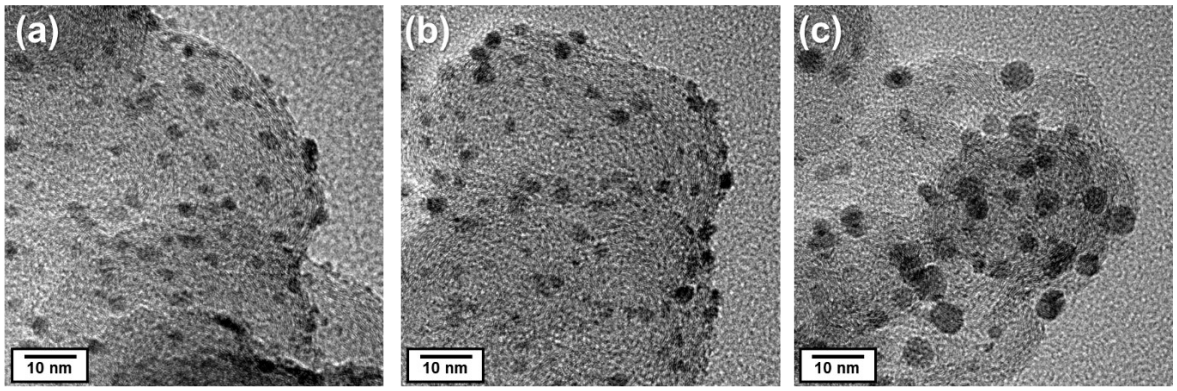

Fig. S1. TEM images of (a) commercial Pt/C, (b) Mn-Pt/C, and (c) Pt_3Mn intermetallic/C.

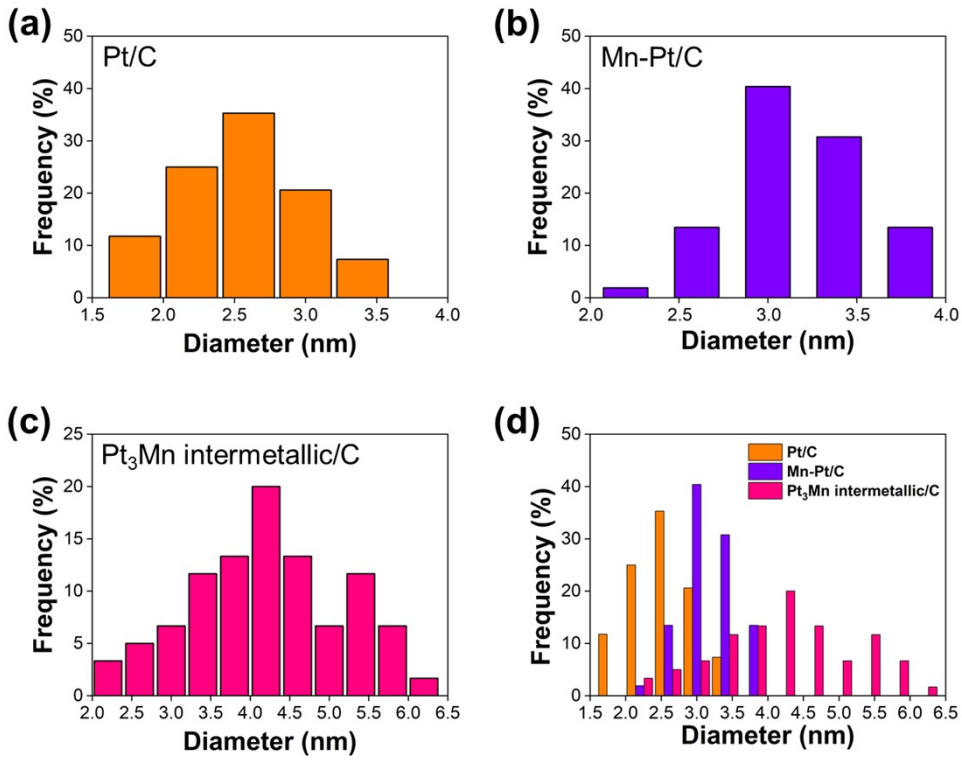

Fig. S2. Particle size distribution of (a) Pt/C, (b) Mn-Pt/C, and (c) Pt_3Mn intermetallic/C. Average particle sizes are 2.55, 3.16, and 4.23 nm for Pt/C, Mn-Pt/C, and Pt_3Mn intermetallic/C. For comparison, particle size distributions of Pt/C, Mn-Pt/C, and Pt_3Mn intermetallic/C are presented in (d).

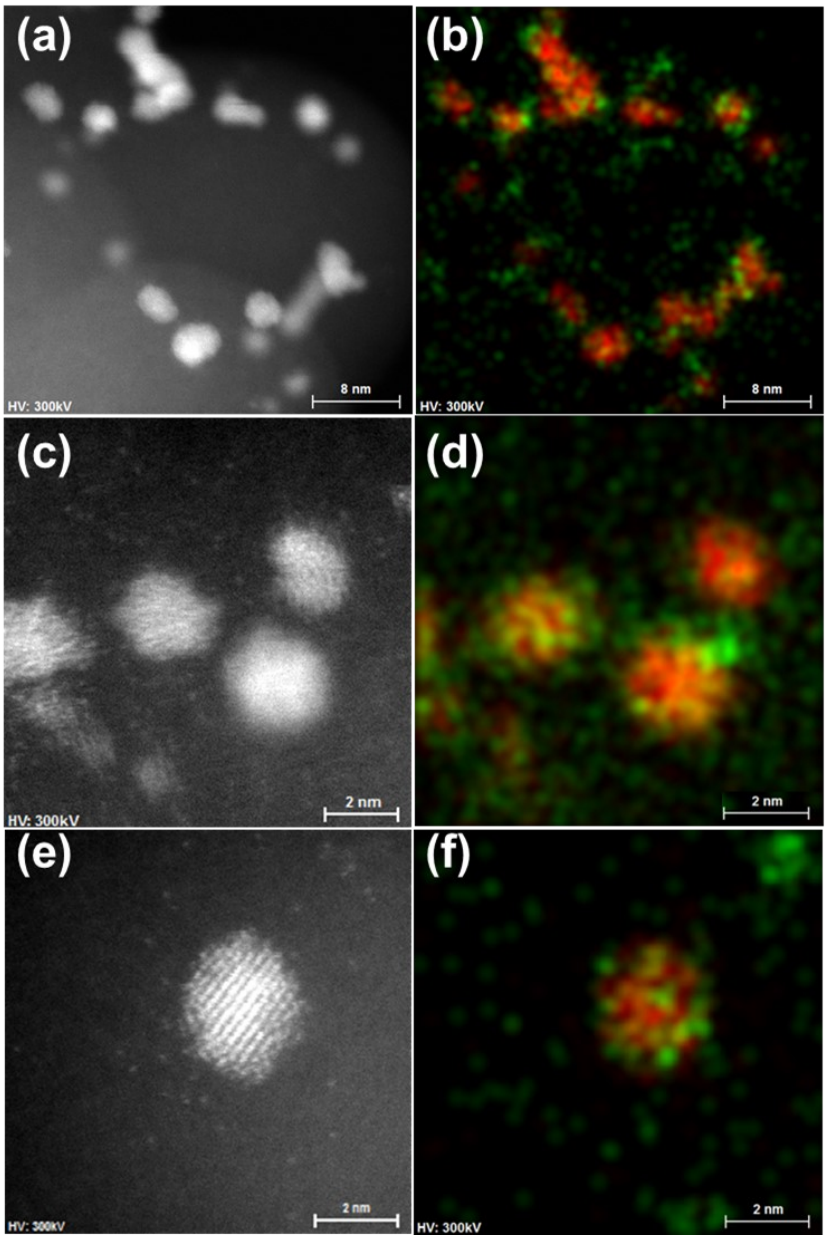

Fig. S3. EDS mapping images of Mn-Pt/C. Mn (green) atoms are mostly observed on Pt (red) nanoparticles.

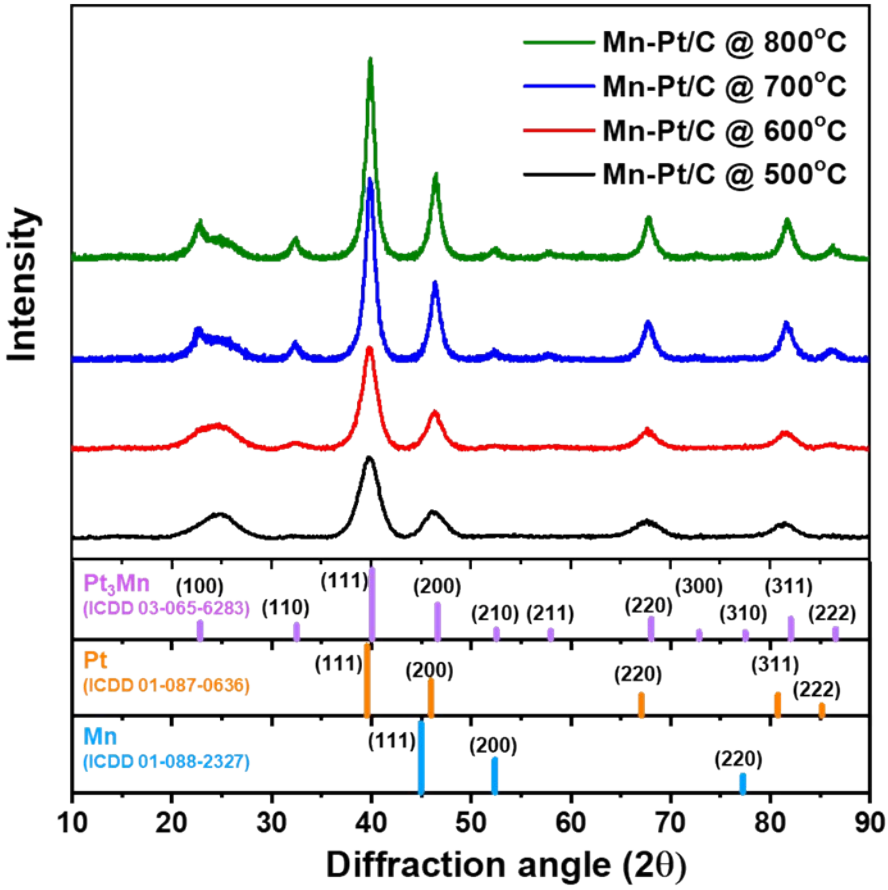

Fig. S4. XRD patterns of Mn-Pt/C annealed at 500, 600, 700, and 800 °C. With an increase in the annealing temperature, the XRD peaks from the Pt_3Mn intermetallic phase are intensified. Pt_3Mn intermetallic/C catalyst was annealed at 700 °C in this work.

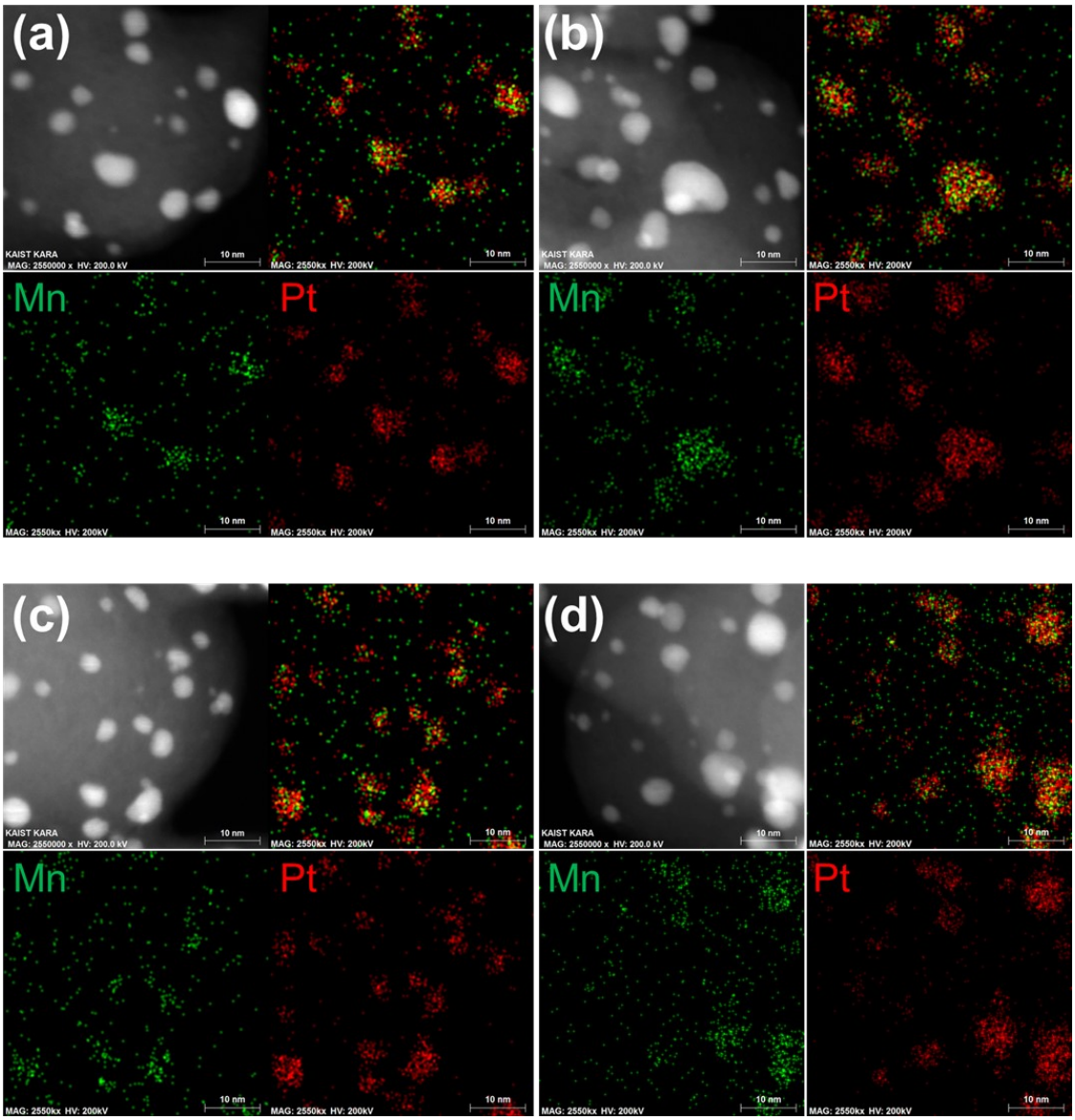

Fig. S5. (a-d) STEM and EDS mapping images of Pt_3Mn intermetallic/C.

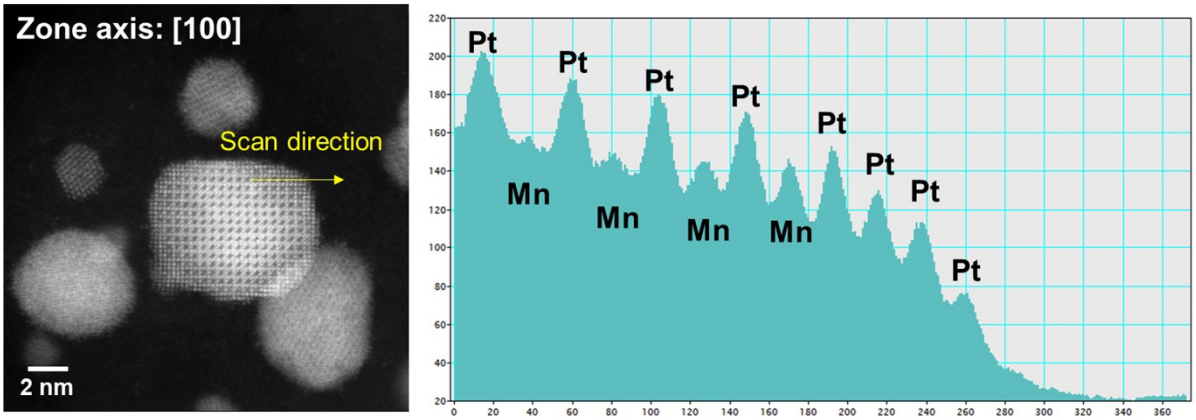

Fig. S6. HR-STEM images and their intensity profiles of Pt_3Mn intermetallic nanoparticles with [100] zone axis.

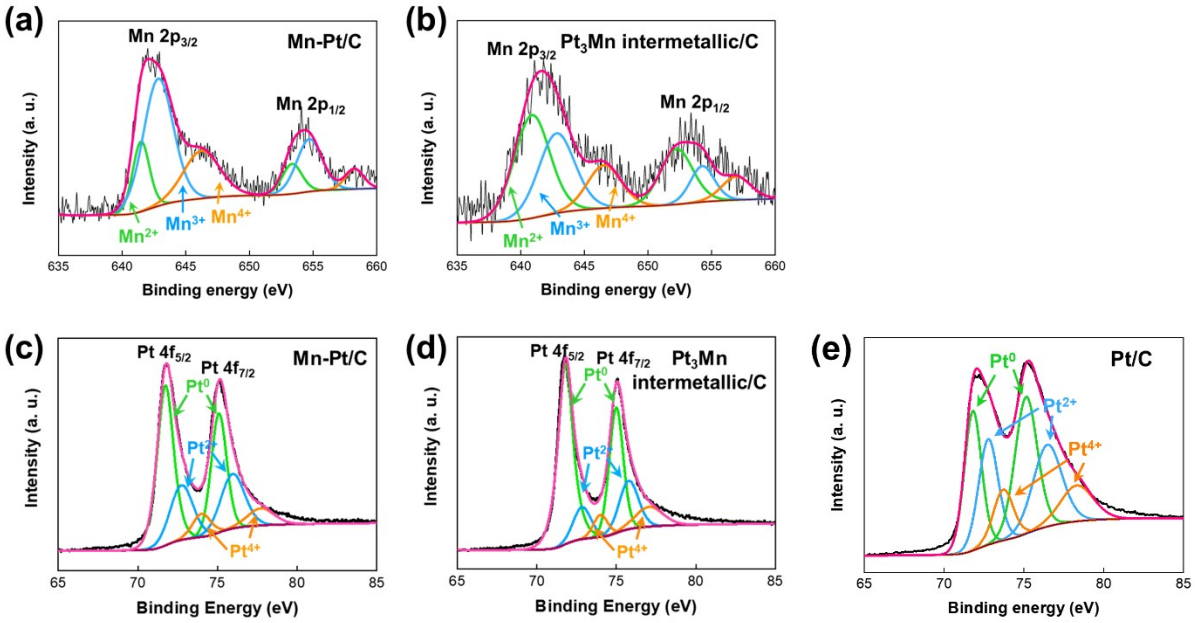

Fig. S7. Mn 2p XPS spectra of (a) Mn-Pt/C and (b) Pt_3Mn intermetallic/C. Pt 4f XPS spectra of (c) Mn-Pt/C, (d) Pt_3Mn intermetallic/C, and (e) Pt/C.

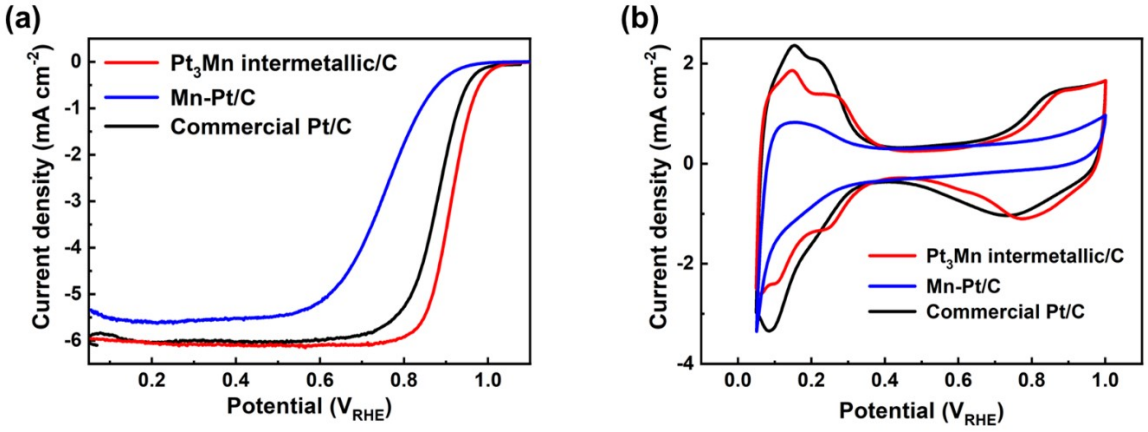

Fig. S8. ORR polarization and CV curves of pristine Pt_3Mn intermetallic/C (700 °C), Mn-Pt/C, and commercial Pt/C catalysts.

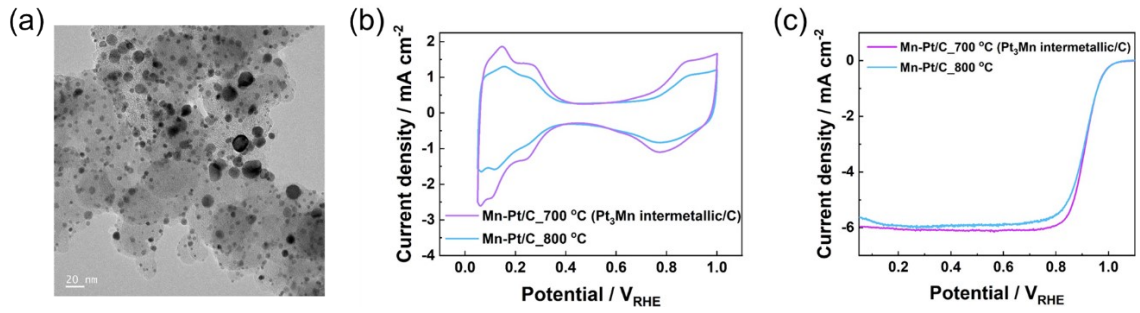

Fig. S9. (a) TEM image of Mn-Pt/C annealed at 800 °C under Ar/H_2 reductive environment for 4 hours (Mn-Pt/C_800 °C). (b) Cyclic voltammograms and (c) ORR polarization curves of Mn-Pt/C_800 °C and Mn-Pt/C_700 °C (Pt_3Mn intermetallic/C). The values of ECSAs, mass activity, and specific activity are summarized in **Table S3**.

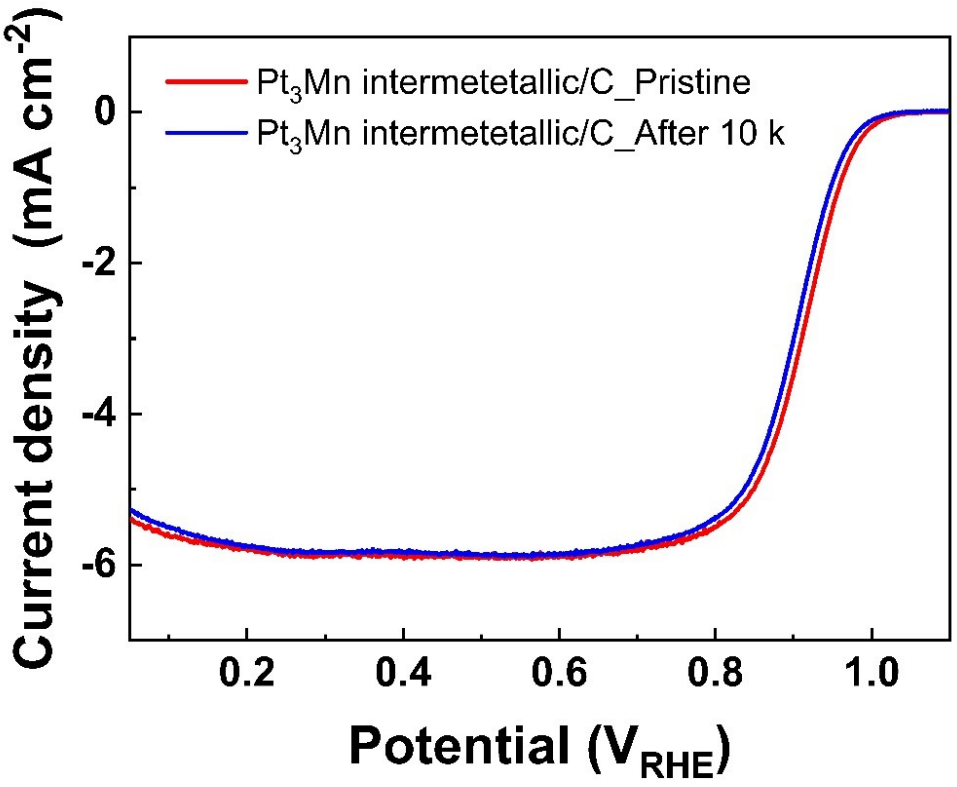

Fig S10. ORR polarization curves of Pt_3Mn intermetallic/C and commercial Pt/C catalysts before and after 10 k ADT potential cycling test in 0.1 M $HClO_4$ solution.

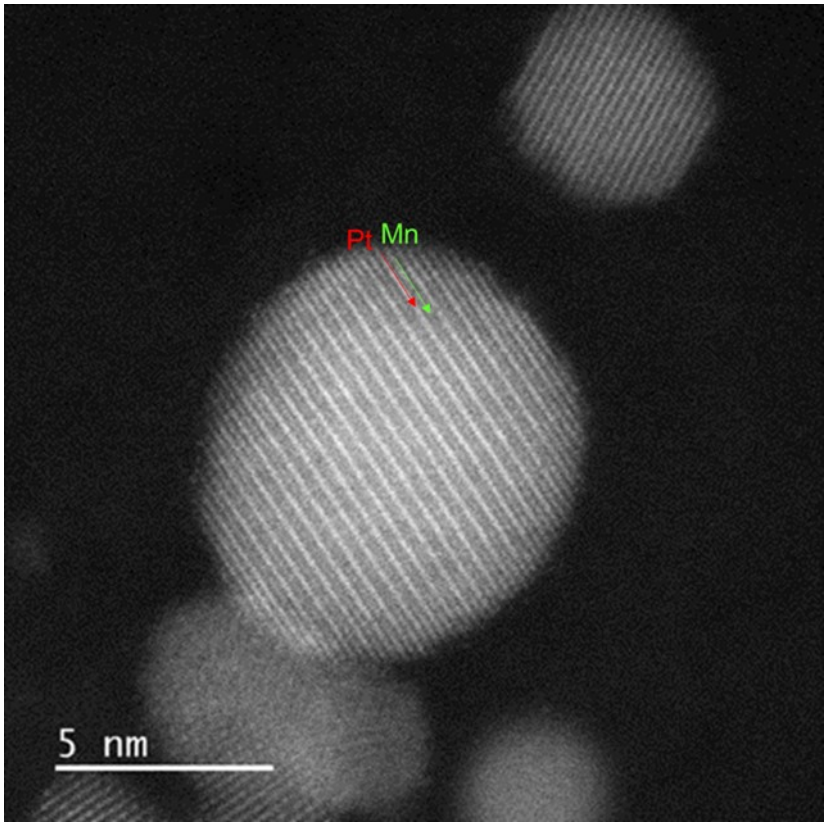

Fig. S11. STEM image of Pt_3Mn intermetallic nanoparticle after 10k cycles.

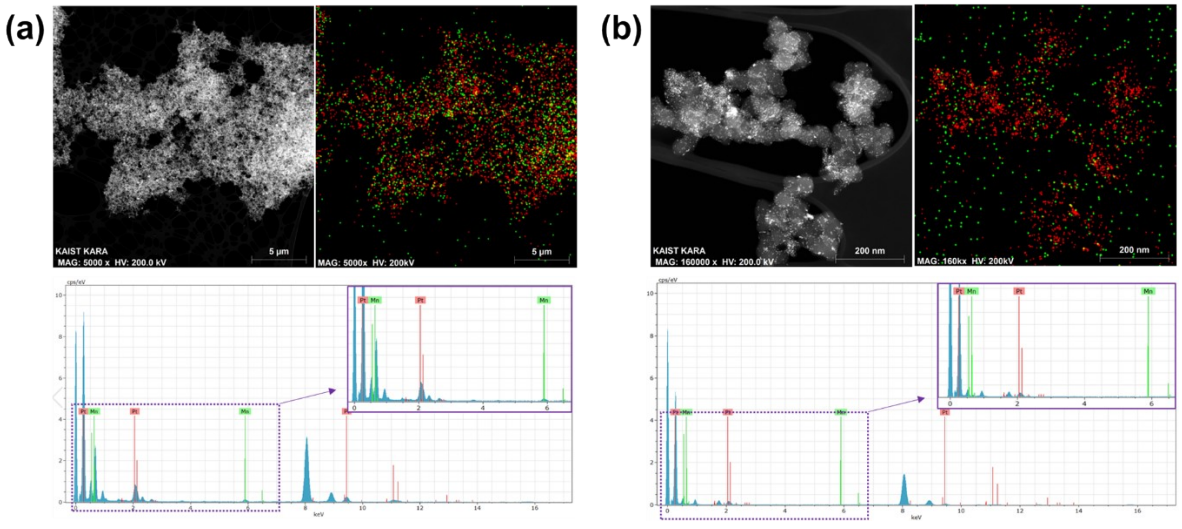

Fig. S12. Low magnification EDS mapping images of (a) Pt_3Mn intermetallic and (b) Mn-Pt/C after 10k cycles. Corresponding chemical compositions are summarized in **Table S4**.

Table S1. Chemical composition of Mn-Pt/C and Pt_3Mn intermetallic/C measured using ICP-OES (at%).

	Mn-Pt/C	Pt_3Mn intermetallic/C (pristine)	Pt_3Mn intermetallic/C (after RDE 10k cycles)
Pt	75.2	75.1	74.7
Mn	24.8	24.9	25.3
Pt-to-Mn ratio	3.03	3.02	2.95

Table S2. Mass activity, ECSA, and specific activity of Pt_3Mn intermetallic/C, Mn-Pt/C, and commercial Pt/C. (RDE results)

	Mass activity [A mg_{Pt}^{-1}]	$ECSA_{Hupd}$ [m^2 g_{Pt}^{-1}]	Specific activity [mA cm^{-2}]
Pt_3Mn intermetallic/C	0.386	44	0.877
Mn-Pt/C	0.014	30	0.047
Commercial Pt/C	0.125	62	0.202

Table S3. ECSA, mass activity (@ 0.9 V_{RHE}) and specific activity (0.9 V_{RHE}) of Mn-Pt/C annealed at 700 °C (Pt_3Mn intermetallic/C) and Mn-Pt/C annealed at 800 °C catalysts. (RDE results)

	$ECSA_{Hupd}$ [$m^2\ g_{Pt}^{-1}$]	Mass activity [$A\ mg_{Pt}^{-1}$]	Specific activity [$mA\ cm^{-2}$]
Mn-Pt/C_700 °C	44	0.386	0.877
Mn-Pt/C_800 °C	38.94	0.312	0.801

Table S4. Chemical composition changes of Pt_3Mn intermetallic/C and Mn-Pt/C after 10k cycles.

Catalyst after 10k cycles (RDE)	wt%		at%	
	Mn	Pt	Mn	Pt
Pt_3Mn intermetallic/C	7.62	92.38	22.65	77.35
Mn-Pt/C	0.81	99.19	2.83	97.17

Table S5. Concentrations of Pt and Mn in the electrolytes dissolved from Pt_3Mn intermetallic/C and Mn-Pt/C during 10k potential cycles. (ICP-MS, unit: ppb = μg/L).

	Mn	Pt
Blank	0.048	0.015
Pt_3Mn intermetallic/C	38.757	0.650
Mn-Pt/C	205.477	4.213

Table S6. Numbers of Pt atoms and Mn atoms in each sublayer of the slabs.

Layer		**Slab (1)**		**Slab (2)**		**Slab (3)**		**Slab (4)**	
		Pt	Mn	Pt	Mn	Pt	Mn	Pt	Mn
Pt-skin		4	0	4	0	4	0	4	0
Sub-surface	1st	4	0	3	1	2	2	1	3
	2nd	2	2	3	1	4	0	4	0
	3rd	3	1	3	1	3	1	4	0
	4-5th	3	1	3	1	3	1	3	1

Table S7. Single-cell performance of representative Pt-based intermetallic ORR catalysts.

Catalyst	Operating Condition		Loading C/A (mg_{Pt} cm^{-2})	Voltage (V)	Current Density (mA cm^{-2})	Power Density (W cm^{-2})	Ref.
	Gas	Back pressure					
Pt_3Mn intermetallic/C	**H_2-Air (1.5:2.0)**	**No backpressure**	**0.15 / 0.15**	**0.7**	**550**	**0.38**	**This work**
fcc-PtFe/C	H_2-Air (1.5:8.0)	No backpressure	0.2 / 0.2	0.7	~300	~0.21	3
MOF-derived Pt_3Co	H_2-Air	1.5 bar_{abs}	0.13 / N/A	0.8	270	0.22	4
$L1_0$-CoPt/Pt	H_2-Air (500/1000 sccm)	1.5 bar_{abs}	0.105 / N/A	0.7	~700	0.49	5

Computational Details

We performed DFT calculations using the Vienna Ab initio Simulation Package (VASP), in which a plane-wave basis set is employed.[6–9] The kinetic energy cutoff was set to 500 eV to expand the plane wave. The generalized gradient approximation (GGA) was used to describe the exchange-correlational interactions with the Perdew-Burke-Ernzerhof (PBE) functional.[10] The projector-augmented wave method was used to treat core and valence electrons.[11] To describe the oxygen reduction reaction on the intermetallic Pt_3Mn and Pt, we modeled the (111) surfaces of periodically repeated 2×2 supercells with 6 atomic layers and a vacuum width of 15 Å. Pt_3Mn (111) was modeled by a so-called Pt-skin structure, where the outermost layer of 6 atomic layers was composed of only platinum atoms and the two bottom-most layers were fixed for both Pt_3Mn and Pt. The Brillouin zone was sampled with a 4 × 4 × 1 Monkhorst−Pack k-point mesh. The geometries were optimized until the Hellmann-Feynman forces were less than 10^{-2} eV/Å, and the electronic structures were relaxed with a convergence criterion of 10^{-5} eV. An implicit solvation model was implemented to describe the solvent effect by using VASPsol.[12]

In this study, the free energy changes of each step were calculated based on a computational hydrogen electrode model reported by Nørskov et al.[13] Adding entropy term (TΔS) and zero-point energy (ZPE) corrections to the DFT-calculated energies, we could obtain the Gibbs free energy diagram as follows:

$$\Delta G = \Delta E_{DFT} + \Delta ZPE - T\Delta S - neU,$$

where ΔE_{DFT} is the change in the total energy calculated by DFT method; ΔZPE is the difference in zero-point energy; ΔS is the change in entropy; T is temperature, which was set

to the room temperature (298.15K); n is the number of electrons involved in each ORR reaction step; and U is the electrode potential.

The dissolution potential of Pt atoms was calculated as

$$U_{dissolution} = U_{dissolution}^{Bulk\ Pt} + \frac{1}{2n_{dissolved}}\left\{E(Pt_{n-n_{dissolved}}M_m) + n_{dissolved}E(Pt_{bulk}) - E(Pt_nM_m)\right\},$$

where $U_{dissolution}$ and $U_{dissolution}^{Bulk\ Pt}$ are the dissolution potentials of a surface and bulk Pt into Pt^{2+}. Here, we calculated $U_{dissolution}^{Bulk\ Pt}$ as 1.188 V, and $n_{dissolved}$ is defined as the number of Pt atoms dissolved.

REFERENCES

1 G. Zhang, C. Li, J. Liu, L. Zhou, R. Liu, X. Han, H. Huang, H. Hu, Y. Liu and Z. Kang, *J. Mater. Chem. A*, 2014, **2**, 8184–8189.

2 C. Yao, F. Li, X. Li and D. Xia, *J. Mater. Chem.*, 2012, **22**, 16560–16565.

3 D. Y. Chung, S. W. Jun, G. Yoon, S. G. Kwon, D. Y. Shin, P. Seo, J. M. Yoo, H. Shin, Y.-H. Chung, H. Kim, B. S. Mun, K.-S. Lee, N.-S. Lee, S. J. Yoo, D.-H. Lim, K. Kang, Y.-E. Sung and T. Hyeon, *J. Am. Chem. Soc.*, 2015, **137**, 15478–15485.

4 X. X. Wang, S. Hwang, Y.-T. Pan, K. Chen, Y. He, S. Karakalos, H. Zhang, J. S. Spendelow, D. Su and G. Wu, *Nano Lett.*, 2018, **18**, 4163–4171.

5 J. Li, S. Sharma, X. Liu, Y.-T. Pan, J. S. Spendelow, M. Chi, Y. Jia, P. Zhang, D. A. Cullen and Z. Xi, *Joule*, 2019, **3**, 124–135.

6 G. Kresse and J. Furthmüller, *Phys. Rev. B*, 1996, **54**, 11169.

7 G. Kern, G. Kresse and J. Hafner, *Phys. Rev. B*, 1999, **59**, 8551.

8 G. Kresse and J. Furthmüller, *Comput. Mater. Sci.*, 1996, **6**, 15–50.

9 G. Kresse and J. Hafner, *Phys. Rev. B*, 1993, **48**, 13115–13118.

10 J. P. Perdew, K. Burke and M. Ernzerhof, *Phys. Rev. Lett.*, 1996, **77**, 3865–3868.

11 P. E. Blöchl, *Phys. Rev. B*, 1994, **50**, 17953–17979.

12 K. Mathew, R. Sundararaman, K. Letchworth-Weaver, T. A. Arias and R. G. Hennig, *J. Chem. Phys.*, 2014, **140**, 84106.

13 J. K. Nørskov, J. Rossmeisl, A. Logadottir, L. Lindqvist, J. R. Kitchin, T. Bligaard and H. Jonsson, *J. Phys. Chem. B*, 2004, **108**, 17886–17892.